Natural Hazards (2026) 122:258
https://doi.org/10.1007/s11069-025-07967-w

ORIGINAL PAPER

SPT-based liquefaction hazard map using GIS: a case study in Yıldırım district of Bursa, Turkey

Ahmet Talha Gezgin[1] · **Onur Gurbuz**[1]

Received: 19 May 2025 / Accepted: 29 December 2025
© The Author(s) 2025

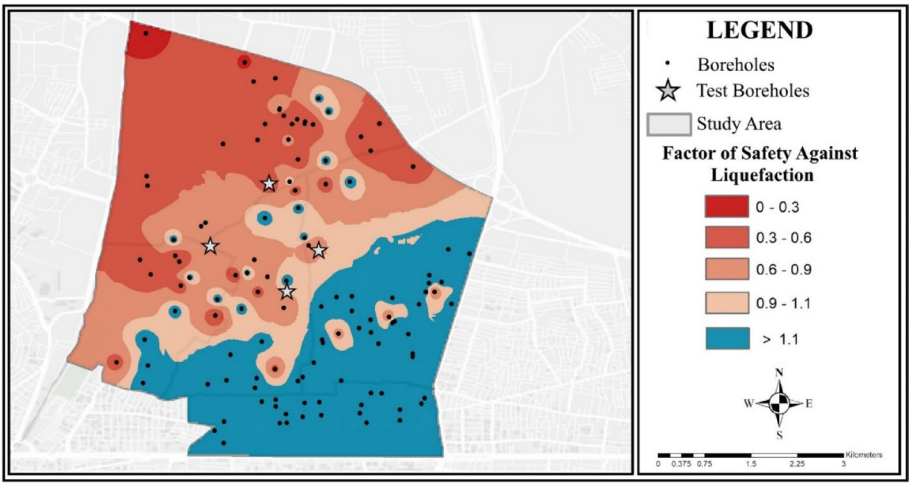
Abstract

This study aims to assess the liquefaction potential in five neighborhoods (Millet, Vatan, Yunusemre, Duaçınarı, and Kazımkarabekir) in the Yıldırım district of Bursa province and to produce GIS-based liquefaction hazard maps. The analyses are carried out based on the Turkish Building Earthquake Code (Turkish Building Earthquake Code, 2018) for a design earthquake scenario with a magnitude of M_w = 7.5 and a return period of 475 years. Standard Penetration Test (SPT) data and laboratory test results obtained from 123 boreholes are used in this study. Evaluations are performed for two different groundwater level conditions: the current level and the most unfavorable level (where groundwater is assumed to reach the surface). The results are spatially interpreted in ArcGIS using IDW interpolation. The findings indicate that the risk of liquefaction is low under current conditions, particularly in southern regions. However, it is revealed that the risk increases significantly in all regions if groundwater rises to the surface. Error analyses are also conducted in the study, comparing the mean error, RMSE, and relative error values using different numbers of boreholes. Accordingly, the effect of borehole distribution on the results is investigated using an epistemic uncertainty approach, revealing that more homogeneous distributions and data densities around 100 boreholes provide relatively more reliable results. These findings reveal that liquefaction risk analyses must consider not only the variability in the groundwater level but also the uncertainties associated with data density and distribution. They also demonstrate that the maps obtained can serve as an important decision support tool in urban planning and disaster risk reduction efforts.

Extended author information available on the last page of the article

Published online: 02 March 2026

Graphical abstract



Keywords Epistemic uncertainty · Error analysis · Geographic information systems (GIS) · Liquefaction hazard mapping · Liquefaction analysis based on standard penetration test · Turkish building earthquake code (TBEC)

1 Introduction

Bursa province is considered one of the important regions where liquefaction-related risks can be observed due to its location and soil structure. Historically, although the city was first established at the base of Uludağ, it has expanded towards the Bursa Plain over time and has spread to areas with thick alluvial layers (Tabban 2000). The alluvial zones constituting the Bursa Plain have a high soil amplification effect, liquefaction potential, and earthquake-induced settlement risk, which may cause significant engineering problems in terms of construction in the region (Akyol et al. 2002; Başarı 2003). Therefore, it is very important to determine the liquefaction potential in the built-up areas in Bursa Plain.

The Turkish Building Earthquake Code (TBEC) (Republic of Türkiye 2018) defines liquefaction as a significant decrease in shear strength and stiffness in cohesionless or low cohesion (PI < 12%) soils located below the groundwater level and up to 20 m deep from the surface as a result of an increase in pore water pressure due to earthquake shaking. Severe structural damage due to liquefaction has recently occurred in many regions worldwide (Seed and Idriss 1967; Tosun et al. 2011; Cetin et al. 2018). While this phenomenon can lead to sinking, tilting, and collapsing structures with shallow foundations, it causes subsurface structures to rise toward the surface and lose slope stability, resulting in significant engineering risks.

Various methods based on both laboratory and field tests are used to determine liquefaction potential. Cyclic simple shear, cyclic triaxial compression, and cyclic torsion shear tests performed on undisturbed soil samples are the most commonly used laboratory-based methods to evaluate liquefaction behavior (Fardad Amini and Noorzad 2018; Zhuang et al. 2018; Puri et al. 2020; Park et al. 2020; Khashila et al. 2021). Under field conditions, Standard Penetration Test (SPT), Cone Penetration Test (CPT), and Multichannel Analysis of Surface

Waves (MASW) are among the most commonly used tests to determine the liquefaction potential of soils (Aytaş et al. 2023; Poddar et al. 2023; Bayramoğlu and Özel 2024; Ansary et al. 2024). These tests allow the soil's resistance to liquefaction to be assessed directly or indirectly. The Turkish Building Earthquake Code (TBEC 2018) recommends that SPT data should be evaluated together with soil classification parameters such as grain size distribution, water content, and Atterberg limits in liquefaction analyses. These data form the basic data set for GIS-based liquefaction risk analyses. Field and laboratory data are quantified prior to spatial analyses and spread over the study area through interpolation methods, and the regional distribution of liquefaction potential is mapped.

Geographic Information Systems (GIS) are a powerful analysis tool for identifying hazard areas before natural disasters and for spatially assessing impacts afterwards. These systems allow the integration of geological, geotechnical, and environmental data. In this way, especially the mapping and management of ground-based risks can be provided more effectively. In a GIS environment, various interpolation methods are used to spread point data over the entire study area. Inverse Distance Weighted (IDW), Kriging, Natural Neighbor, and Spline methods are the most commonly used methods in the literature (Meshram et al. 2021; Yanto et al. 2022; Shynkarenko et al. 2022; Ali and Rahman 2022; Memisoglu Baykal 2025). These methods are also used to determine the spatial distribution of liquefaction potential based on a limited number of borehole data. Thus, areas with liquefaction risk can be visualized with GIS-based thematic maps, and important outputs can be provided for decision makers.

In this study, liquefaction analyses are performed based on Standard Penetration Test (SPT) data. The soil parameters used in the analyses are based on field and laboratory data obtained from a total of 123 boreholes located in five neighborhoods (Millet, Vatan, Yunusemre, Duaçınarı, and Kazımkarabekir) in Yıldırım district of Bursa province. Liquefaction potential is assessed following the methods defined in the TBEC (Republic of Türkiye 2018). Accordingly, a hypothetical earthquake scenario was defined based on Earthquake Ground Motion Level 2 (DD2) with a moment magnitude (Mw) of 7.5 and a 10% probability of exceedance in 50 years, corresponding to a 475-year recurrence period. Considering possible seasonal fluctuations, two different groundwater level (GWL) scenarios are evaluated in the study: the current GWL situation and the situation representing the most unfavorable condition, where GWL is assumed to be at the surface. Factor of safety (FS) values are calculated for both scenarios, and their spatial distributions are obtained using the IDW method in the GIS environment.

Here, the reliability of the results obtained using the IDW method is also questioned by making error analyses (mean error, absolute error, RMSE, standard deviation, and relative error) through the determined test points. Second, the epistemic uncertainty approach is utilized to reveal the effect of the number of boreholes on the results, and the optimal number of boreholes is discussed. Thus, the study not only presents the spatial distribution of the current situation and the worst-case scenario but also examines the limitations of the method used and the reliability of the data.

This study contributes to the literature by demonstrating how GIS-based methods can be used to prepare liquefaction risk maps at the regional scale, the impact of data density and groundwater level on the results, and how different scenarios can be reflected in engineering decision-making processes.

2 Geographical location and seismicity of the study area

In this study, the study area included five neighborhoods (Millet, Vatan, Yunusemre, Duaçınarı, Kazımkarabekir) of Yıldırım district of Bursa (see Fig. 1). These are spread over a total area of 678 hectares (Atlasbig). The total number of people living in these neighborhoods is 72,509 (Turkish Statistical Institute (TSI) 2025). Bursa is located at the intersection of 40 degrees north parallel and 29 degrees east meridian in the South Marmara section of the Marmara Region. It is surrounded by Bilecik and Sakarya in the east, Kocaeli, Yalova, Istanbul, and the Marmara Sea in the north, Kütahya in the south, and Balıkesir in the west (see Fig. 2). In the eastern parts of Bursa Plain, where the neighborhoods of the study area are located, the alluvium layer varies between 140 m and 200 m and contains fine-grained clay, silt, sand, and gravel-type soils (Tabban 2000; Akyol et al. 2002; Başarı 2003).

Turkey's earthquake hazard maps show that the North Anatolian Fault influences the Bursa province Yıldırım district. Bursa and its surroundings are on one of Turkey's most famous fault zones, the right-lateral, strike-slip North Anatolian Fault, which extends towards western Anatolia. Earthquakes with a high potential to affect Bursa are expected to originate from the Gemlik section of the North Anatolian Fault, Uluabat Fault, and Bursa Fault (see Fig. 3).

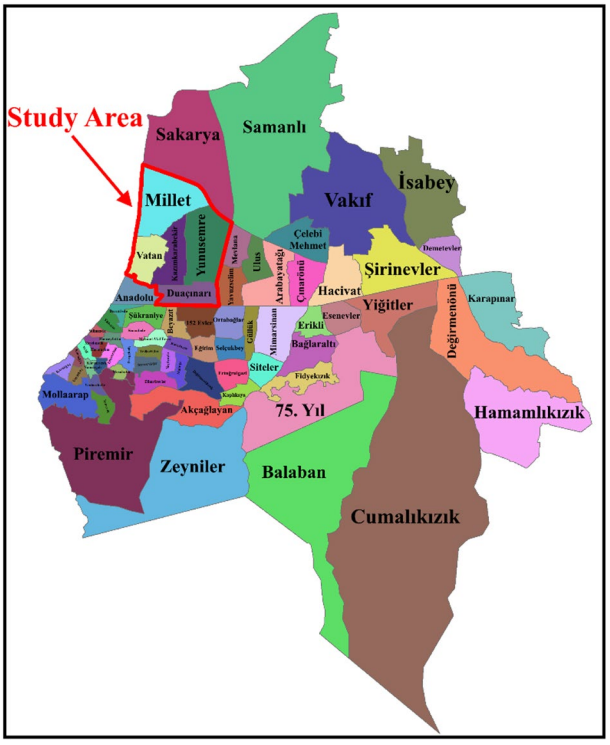


Fig. 1 Study area in the map of the Yıldırım district

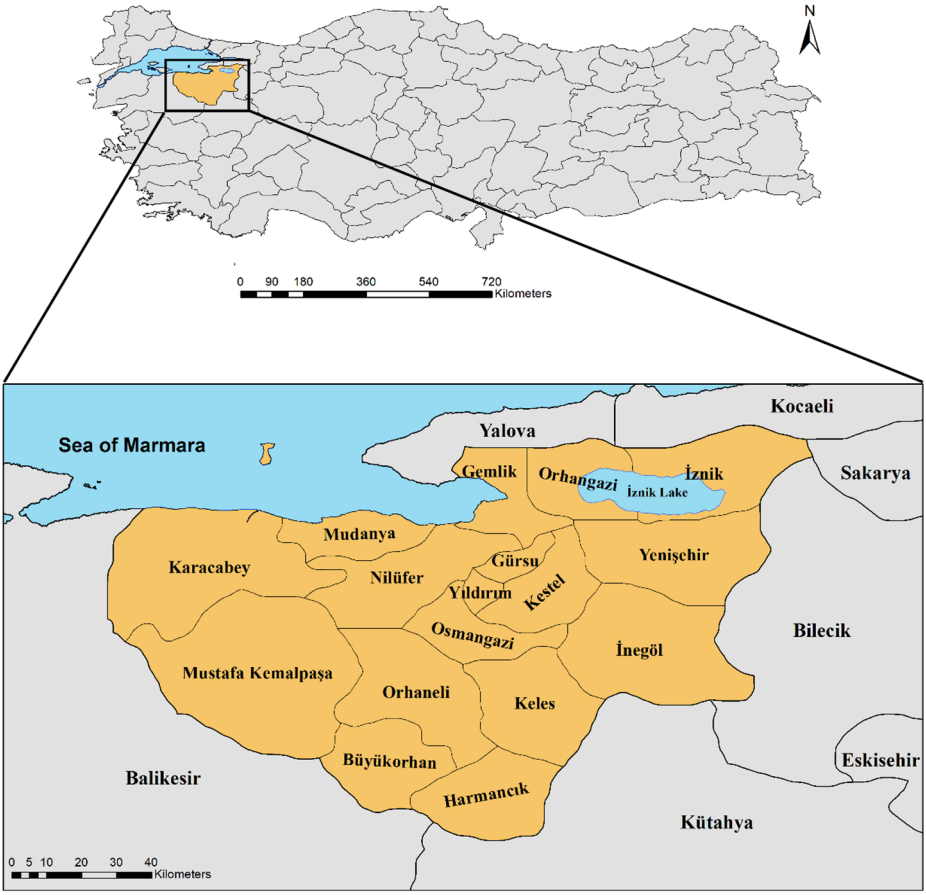


Fig. 2 Location of Bursa city

3 Methodology

3.1 Evaluation of liquefaction potential of soils

This study evaluates the liquefaction potential of soils using SPT data and laboratory test results, following the steps recommended in the Turkish Building and Earthquake Code (TBEC) (Republic of Türkiye 2018) published in 2018. However, the studies that propose the equations used in the steps presented by TBEC (Republic of Türkiye 2018) are also presented in this paper.

The current TBEC (Republic of Türkiye 2018), therefore, this study follows the "Cyclic Stress Approach" for evaluating the liquefaction potential of soil. This approach defines the soil's loading conditions and liquefaction resistance in cyclic shear stresses. The liquefaction potential is assessed by comparing the liquefaction resistance (τ_R) and average cyclic shear stress(τ_{av}) (Kramer and Stewart 2025). TBEC (Republic of Türkiye 2018) defines the safety condition against liquefaction as shown in Eq. (1).

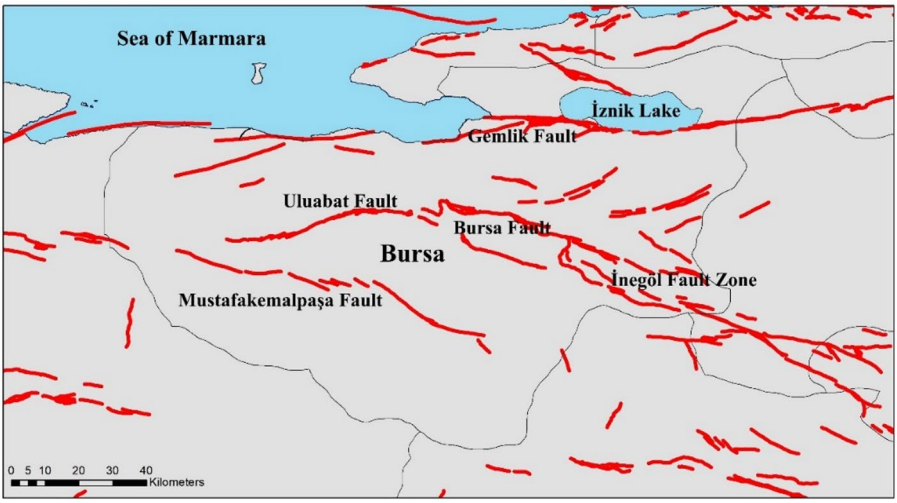


Fig. 3 The faults influencing Bursa and its surroundings

$$\frac{\tau_R}{\tau_{av}} \geq 1.10 \tag{1}$$

3.1.1 Determination of average Cyclic shear stress

Seed and Idriss (1971) derived the following equation in their simplified procedure to estimate the average cyclic shear stress:

$$\tau_{av} = 0.65 \frac{a_{max}}{g} \sigma_{v0} r_d \tag{2}$$

Here, a_{max} is peak ground surface acceleration, g is gravity acceleration, σ_{v0} is total vertical stress, and r_d is stress reduction factor at related depth. σ_{v0} is due to the weight of the soil column above a soil element at depth h. The reduction factor can be calculated for a specific depth using the following Equations.

$$\begin{aligned} &z \leq 9.15\,m \;\rightarrow\; r_d = 1.0 - 0.00765z \\ &9.15\,m < z \leq 23\,m \;\rightarrow\; r_d = 1.174 - 0.0267z \\ &23\,m < z \leq 30\,m \;\rightarrow\; r_d = 0.744 - 0.008z \\ &z > 30\,m \;\rightarrow\; r_d = 0.50 \end{aligned} \tag{3}$$

Here, z is the depth below the ground surface in meters. The first two equations are proposed by Liao and Whitman (1986), and the others by Robertson and Wride (1998). These equations can provide estimates that fit the mean of the range suggested byBolton Seed and Idriss (1971) for the reduction factor.

As seen in Eq. (2), the average cyclic shear stress (τ_{av}) is usually identified as a function of ground motion acceleration at the surface (a_{max}/g) in conventional liquefaction potential evaluation. However, TBEC (Republic of Türkiye 2018) revises this method and

recommends using $0.4 \times S_{DS}$ instead of a_{max}/g. Here, S_{DS} represents the short-period design spectral acceleration coefficient, and this approach aims to consider local soil conditions and regional seismic hazards more comprehensively. The 0.4 coefficient provides a more realistic seismic load assessment in liquefaction analyses by establishing an empirical relationship between S_{DS} and expected maximum acceleration levels. This provides a calculation framework that is more compatible with modern seismic hazard analyses while maintaining consistency with traditional methodologies. This change contributes to current approaches in earthquake engineering by providing more reliable estimates of liquefaction potential. Therefore, this study prefers using 0.4 S_{DS} as the maximum ground motion acceleration at the surface. Here, the S_{DS} coefficient is taken as 1.047.

3.1.2 Determination of liquefaction resistance

Liquefaction resistance (τ_R) is calculated by multiplying the cyclic resistance ratio against an earthquake with a moment magnitude 7.5 ($CRR_{M7.5}$) by the design earthquake moment magnitude correction coefficient (C_M) and the effective vertical stress (σ'_{v0}) as shown in Eq. (4) (Seed and Idriss 1971; Idriss and Boulanger 2008).

$$\tau_R = CRR_{M7.5} C_M \sigma'_{v0} \tag{4}$$

$CRR_{M7.5}$ can be defined as the ratio of the resistance of a soil to shear stresses applied during earthquakes and the effective overburden stress on the soil under earthquakes of magnitude 7.5. $CRR_{M7.5}$ is usually calculated from empirical data obtained from in-situ tests such as standard penetration test (SPT), cone penetration test (CPT), shear wave velocity measurements (Vs), and Becker penetration test (BPT) (Youd and Idriss 2001). This parameter is considered critical to determine whether the soil is at risk of liquefaction for earthquakes with a magnitude of 7.5.

In this study, SPT results are utilized to determine $CRR_{M7.5}$ as suggested in TBEC (Republic of Türkiye 2018). For SPT based $CRR_{M7.5}$ calculation, the number of blows corrected for fine grain content ($N_{1,60f}$) is used as shown in Eq. (5) modified from it proposed by Youd and Idriss (2001) for clean sands.

$$CRR_{M7.5} = \frac{1}{34 - N_{1,60f}} + \frac{N_{1,60f}}{135} + \frac{50}{\left[10 \times N_{1,60f} + 45\right]^2} - \frac{1}{200} \tag{5}$$

It is crucial important that Eq. (5) is valid for only the situation where $N_{1,60f} < 30$. Otherwise, the granular soil is considered to be too dense to liquefy.

The increase in the fine particle content in the sand leads to a rise in the CRR value (Seed et al. 1985). Since the CRR value can be defined as a function of the SPT results, one of the corrections developed for the effect of fines content (FC) on CRR is based on the parameter $N_{1,60}$, the number of SPT impacts (N) normalised to a hammer energy ratio of 60% and a cover pressure of 100 kPa (Seed et al. 1985). Therefore, the effect of fines content (FC) on $N_{1,60}$ is quantified using Eq. (6) (Youd and Idriss 2001).

$$N_{1,60f} = \alpha + \beta N_{1,60} \tag{6}$$

Here, α and β coefficients are dependent on the fine-grain content. When the fine-grain content is less than 5%, $\alpha = 0$ and $\beta = 1$, while $\alpha = 5.0$ and $\beta = 1.2$ for IDI $\geq$ 35%. On the other hand, IDI values were between 5% and 35%, α and β coefficients are calculated using Eqs. 7 and 8, respectively.

$$\alpha = exp\left[1.76 - \left(190/IDI^2\right)\right] \tag{7}$$

$$\beta = 0.99 + IDI^{1.5}/1000 \tag{8}$$

The $N_{1,60}$ value is obtained by adjusting the N value obtained from the SPT test with various corrections. The first one is the energy correction, which is made to adjust the result for differences in the efficiency of the test equipment. The other three corrections are related to hole diameter, sampler type, and rod length. The last correction is associated with the overburden because Gibbs and Holtz (1957) clearly showed that SPT results in sand soil can be affected by overburden pressure. Accordingly, the $N_{1,60}$ value is calculated using Eq. (9).

$$N_{1,60} = NC_EC_BC_SC_RC_N \tag{9}$$

Here C_E is the energy rate correction factor, C_B is the borehole diameter correction factor, C_S is the sampler type correction factor, C_R is the rod length correction factor, and C_N is the overburden correction factor. In this study, C_{B}, C_{S}, and C_{R} are selected from Table 16B.1 in TBEC (Republic of Türkiye 2018), proposed by Robertson and Wride (1998), while C_E factor is revised in TBEC (Republic of Türkiye 2018) according to the conditions in Turkey. For the C_N factor, there are several methods proposed (Teng 1962; Bazaraa 1967; Seed et al. 1975; Tokimatsu and Yoshimi 1983; Liao and Whitman 1986). In this study, Eq. (10) proposed by Liao and Whitman 1986) is used to determine the C_N factor, where σ'_{v0} is the effective vertical stress at the depth of the test.

$$C_N = 9.78\sqrt{\frac{1}{\sigma'_{v0}}} \leq 1.70 \tag{10}$$

Several correction factors, called "magnitude scaling factor (C_M)", have been developed to determine the liquefaction resistance of a soil exposed to an earthquake with a magnitude greater than or less than 7.5 (Seed and Idriss 1982; Idriss 1990; Arango 1996; Idriss and Boulanger 2008). TBEC (Republic of Türkiye 2018) advises the magnitude scaling factor shown in Eq. (11), which Idriss (1990) proposed in his H.B. Seed memorial lecture.

$$C_M = \frac{10^{2.24}}{M_w^{2.56}} \tag{11}$$

According to Eq. (4), the last parameter required for the calculation of liquefaction resistance is the effective stress at the relevant depth. For the computation of the effective stress, the unit weights of the soil units that vary up to the considered depth and the groundwater table are necessary. In this study, the liquefaction resistance is aimed to be calculated under the conditions of both the current groundwater level and the GWT at the surface, which represents the worst condition. Therefore, the effective stress values calculated for two different

GWT conditions also vary. Considering the GWT-dependent fluctuations in the effective stress is highly important.

3.2 Borehole-based liquefaction analysis procedure

This study uses data from 123 boreholes from Yıldırım Municipality to determine the liquefaction potential. The borehole data include groundwater level, SPT blow counts, and fine-grain content. The data are analyzed at every 1.5 m depth interval to the extent that the available data files allow.

In the first stage, SPT blow counts, fines contents, and effective stress values are listed for each borehole at depths up to 20 m. It is also noted whether each depth is below the GWT or not. In the next step, the safety factors (FS) against liquefaction at different depths were calculated at each drilling location by following the steps described in Sect. 3.1. The FS values are obtained as a ratio of the calculated liquefaction resistances to the average cyclic shear stresses. For each borehole, the smallest FS values calculated for different depths are accepted as the FS for the borehole. This method ensures that each point represents the most critical liquefaction potential.

Following this process, a data set is created regarding the safety factors against liquefaction for both the GWT conditions (current and surface levels) throughout the study area. This data set constitutes a basic infrastructure for spatial analyses and map-based interpretations.

3.3 Spatial mapping of liquefaction potential

Geographic Information Systems (GIS) is a computer-aided system developed to map and analyse surface shapes and events occurring on the Earth's surface. GIS is widely used in many sectors such as urban and regional planning, agriculture, forestry, landscape planning, geology, defence, security, tourism, archaeology, local governments, population studies, education, environmental management, and medicine. It is also frequently used to produce liquefaction hazard maps of a specific region (Sitharam et al. 2007; Mhaske and Choudhury 2010; Bourenane et al. 2018; Rawat et al. 2022; Sett et al. 2023).

Since it is not economically and practically feasible to collect data from every point of the study area, GIS-based studies often utilize interpolation methods. Accordingly, this study aims to estimate the spatial distribution for the whole area based on sample data collected from different locations. Several techniques, such as Inverse Distance Weighted (IDW), Kriging, Natural Neighbour, Spline, and Trend, can be used for interpolation in a GIS environment.

This study uses the Inverse Distance Weighted (IDW) method using the GIS-based ArcGIS 10.8 program. The IDW method estimates the values at unsampled points based on the values at sampled points. As the distance increases, the effect of sample points decreases. The IDW method estimates the values using Eq. (12) (Burrough et al. 2015).

$$z\left(x_0\right)=\frac{\sum_{i=1}^{n} z\left(x_i\right) d_{i_0}^{-\Gamma}}{\sum_{i=1}^{n} d_{i_0}^{-\Gamma}} \tag{12}$$

Here, x_0 is the predicted location, n is the number of neighboring measurement locations, Γ is the weight exponent parameter, d_{i0} is the distance between the prediction and measurement point.

Accordingly, liquefaction risk maps are generated for two different locations of the groundwater table (current state and surface level). Furthermore, thematic maps showing the distribution of SPT-N values at different depths and the groundwater level in the study area are also prepared. In this way, it is aimed to evaluate the difference between the liquefaction risk maps to be presented for two different GWT conditions in a more meaningful way.

3.4 Analysis of errors in IDW interpolation

It is known that interpolation analyses contain errors based on estimates between values based on known data. Accordingly, error analysis is made to evaluate the accuracy of data created with the IDW (Inverse Distance Weighting) interpolation method and to determine the uncertainties in the estimates. For this purpose, four borehole points located in the center of the study area are extracted from the IDW analysis data. The estimated values obtained for these points as a result of the analysis are compared with the actual measurements. Thus, the estimation power and potential deviations of the interpolation method are quantitatively revealed. Error metrics (error, absolute error, square of error, and relative error) are calculated using Eqs. (13)–(16).

$$Error_i = Measured\,FS_i - Calculated\,FS_i \tag{13}$$

$$|Error_i| = |Measured\,FS_i - Calculated\,FS_i| \tag{14}$$

$${Error_i}^2 = (Measured\,FS_i - Calculated\,FS_i)^2 \tag{15}$$

$$Rel.Error_i = \frac{|Measured\,FS_i - Calculated\,FS_i|}{Measured\,FS_i} \times 100\% \tag{16}$$

However, summary error statistics are calculated using Eqs. (17)–(21), respectively.

$$ME = \frac{1}{n}\sum {}^{n}_{i=1} Error_i \tag{17}$$

$$MAE = \frac{1}{n}\sum {}^{n}_{i=1} |Error_i| \tag{18}$$

$$MSE = \frac{1}{n}\sum {}^{n}_{i=1} {Error_i}^2 \tag{19}$$

$$RMSE = \sqrt{MSE} \tag{20}$$

$$SD = \sqrt{\frac{1}{n-1}\sum {}^{n}_{i=1}(Error_i - ME)^2} \tag{21}$$

Here, ME is mean error, MAE is mean absolute error, MSE is mean squared error, RMSE is root mean squared error, and SD is standard deviation. The error analysis considered different hydrological scenarios (e.g., rising groundwater levels) and examined their effects on the interpolation results. Increasing error values indicate uncertainty arising from scenario assumptions. This approach reveals both the reliability of IDW interpolation and the potential uncertainties in the estimates.

3.5 Evaluating epistemic uncertainty for optimum borehole distribution

The number of data points used in interpolation analyses and their spatial distribution have a direct impact on the reliability of the results. Therefore, the epistemic uncertainty of the results obtained using the IDW method is evaluated based on different numbers of borehole points. In the analysis, a certain number of borehole points (19, 39, and 59, respectively) are extracted from the existing 119 Borehole points before repetition of the IDW analyses. When determining the borehole points to be extracted, they are selected from areas with high density. In this way, it is aimed to obtain as homogeneous a distribution as possible within the study area.

IDW interpolation is performed again for each scenario, error analyses are conducted on test borehole points using the cross-validation method, and error metrics (MAE, RMSE, and SD) are calculated. The change in error values is observed as the number of boreholes decreases, and the optimum number of boreholes is considered to be obtained at the point where the error statistics do not fall below a certain threshold value. This approach reveals epistemic uncertainty by considering the distribution characteristics of field data and provides a guiding framework for more efficient drilling planning.

4 Results

4.1 Liquefaction potential calculations on a sample borehole location

In this section, the liquefaction analysis steps performed for a sample borehole located in Yıldırım district are presented in detail. The calculations were performed every 1.5 m in the depth range of 0.0–19.5 m. The analysis process is structured through Tables 1, 2, 3 and 4.

Table 1 contains the basic geotechnical parameters of the soil. These parameters consist of dry unit volume weight, saturated unit volume weight, fine content, plasticity index, and

Table 1 Soil parameters at a borehole example

Depth (m)	1.5	3.0	4.5	6.0	7.5	9.0	10.5	12.0	13.5	15.0	16.5	18.0	19.5
γ_{dry} (kN/m^3)	15	15	16	16	16	16	17	17	17	17	17	18	18
γ_{sat} (kN/m^3)	16	16	17	17	17	17	18	18	18	18	18	19	19
IDI (%)	36	19	22	14	17	21	27	24	19	21	22	16	27
PI (%)	9	4	10	14	11	18	8	7	10	14	11	14	17
N (−)	9	6	9	14	10	17	22	24	28	32	37	43	48

Table 2 Parameters required to calculate the average Cyclic shear stress for both GWT conditions

Depth (m)	1.5	3.0	4.5	6.0	7.5	9.0	10.5	12.0	13.5	15.0	16.5	18.0	19.5
Independent of the GWT level													
S_{DS} (−)	1.047	1.047	1.047	1.047	1.047	1.047	1.047	1.047	1.047	1.047	1.047	1.047	1.047
r_d (−)	0.99	0.98	0.97	0.95	0.94	0.93	0.89	0.85	0.81	0.77	0.73	0.69	0.65
GWT at −10 m													
σ_{v0} kPa	22.5	45.0	72.0	96.0	120.0	144.0	179.0	206.0	233.0	260.0	287.0	332.0	360.5
GWT at the surface													
σ_{v0} kPa	24.0	48.0	76.5	102.0	127.5	153.0	189.0	216.0	243.0	270.0	297.0	342.0	370.5

SPT-N values. These data constitute the first step of the analysis process, since they are directly used to calculate both liquefaction resistance and average cyclic shear stress.

Table 2 presents the parameters used in the calculation of the average cyclic shear stress (τ_{av}) and the results obtained with the help of these parameters. S_{DS} and r_d parameters are independent from the level of groundwater table. Here, the one parameter depending on the GWT level is the vertical total stress (σ_{v0}) since the unit volume weights of soil layers vary according to whether they are saturated with water or not. Therefore, the vertical total stresses at different depths are calculated for both the existing groundwater level condition and the worst-case scenario where the groundwater level is assumed to be in the same plane as the surface. Thus, the average cyclic shear stress (τ_{av}) at the different depths varying from 1.5 m to 19.5 m can be determined under different water level conditions to consider the effect of seasonal fluctuations.

On the other hand, Table 3 contains the calculation steps for liquefaction resistance for a borehole sample. Accordingly, the parameters are evaluated as independent and dependent on the groundwater level, as is performed for Table 2. Accordingly, the groundwater level has no effect on the coreection factors (C_E, C_B, C_S, C_R) used to obtain corrected SPT-N values (N_{60}) based on energy and manufacturing. However, the groundwater level has a significant effect on the overburden-corrected SPT stroke numbers ($N_{1,60}$). The reason for this effect is that the overburden correction factor (C_N) depends on the vertical effective stress value. The reason for this effect is that the overburden correction factor depends on the vertical effective stress value. The effective stress impact on the C_N factor affects the value of $N_{1,60f}$ and subsequently the $CRR_{M7.5}$ value, which is an important parameter of the liquefaction resistance calculation, as shown in Eq. (4). In summary, the vertical effective stresses calculated at different depths have both direct and indirect (through the $CRR_{M7.5}$ value) effect on the liquefaction resistance calculation. As a result, Table 3 presents the parameters used in the calculation of liquefaction resistances for both groundwater levels.

As seen in Eq. (4), soil layers exhibit different liquefaction resistances against earthquakes of different magnitudes. This effect on the resistance is described by the C_M coefficient calculated as shown in Eq. (11). Since this study aims to calculate the liquefaction resistance in response to a magnitude 7.5 earthquake as recommended in TBEC (Republic of Türkiye 2018), the C_M coefficient is defined as 1.

Additionally, Table 3 shows that the $CRR_{M7.5}$ value at 19.5 m depth is negative when the groundwater level is at the surface. It is specifically noted that there are no calcula-

Table 3 Parameters required to calculate the liquefaction resistance for both GWT conditions

Depth (m)	1.5	3.0	4.5	6.0	7.5	9.0	10.5	12.0	13.5	15.0	16.5	18.0	19.5
Independent of the GWT level													
C_E (−)	0.75	0.75	0.75	0.75	0.75	0.75	0.75	0.75	0.75	0.75	0.75	0.75	0.75
C_B (−)	1.00	1.00	1.00	1.00	1.00	1.00	1.00	1.00	1.00	1.00	1.00	1.00	1.00
C_S (−)	1.00	1.00	1.00	1.00	1.00	1.00	1.00	1.00	1.00	1.00	1.00	1.00	1.00
C_R (−)	0.75	0.75	0.85	0.85	0.95	0.95	1.00	1.00	1.00	1.00	1.00	1.00	1.00
N_{60} (−)	5.1	3.4	5.7	8.9	7.1	12.1	16.5	18.0	21.0	24.0	27.8	32.3	36.0
α (−)	5.00	3.43	3.93	2.20	3.01	3.78	4.48	4.18	3.43	3.78	3.93	2.77	4.48
β (−)	1.20	1.07	1.09	1.04	1.06	1.09	1.13	1.11	1.07	1.09	1.09	1.05	1.13
C_M (−)	1	1	1	1	1	1	1	1	1	1	1	1	1
GWT at −10 m													
σ'_{v0} (kN/m^2)	22.5	45.0	72.0	96.0	120.0	144.0	174.1	186.4	198.7	211.0	223.3	253.6	267.4
C_N (−)	1.70	1.70	1.15	1.00	0.89	0.82	0.74	0.72	0.69	0.67	0.65	0.61	0.60
$N_{1,60}$ (−)	8.6	5.7	6.6	8.9	6.4	9.9	12.2	12.9	14.6	16.2	18.2	19.8	21.5
$N_{1,60f}$ (−)	15.3	9.6	11.2	11.5	9.8	14.5	18.3	18.5	19.1	21.3	23.8	23.6	28.8
$CRR_{M7.5}$ (−)	0.16	0.11	0.12	0.13	0.11	0.16	0.20	0.20	0.20	0.23	0.27	0.27	0.40
GWT at the surface													
σ'_{v0} (kN/m^2)	9.3	18.6	32.4	43.2	54.0	64.8	86.1	98.4	110.7	123.0	135.3	165.6	179.4
C_N (−)	1.70	1.70	1.70	1.49	1.33	1.21	1.05	0.99	0.93	0.88	0.84	0.76	0.73
$N_{1,60}$ (−)	8.6	5.7	9.8	13.3	9.5	14.7	17.4	17.7	19.5	21.2	23.3	24.5	26.3
$N_{1,60f}$ (−)	15.3	9.6	14.6	16.0	13.1	19.8	24.1	23.8	24.4	26.8	29.4	28.6	34.2
$CRR_{M7.5}$ (−)	0.16	0.11	0.16	0.17	0.14	0.21	0.28	0.27	0.28	0.33	0.43	0.39	NL

tion errors here. As specifically stated by Youd and Idriss (2001), the calculation of the $CRR_{M7.5}$ parameter using Eq. (5) is only valid when the $N_{1,60f}$ value is less than 30. However, it is seen that the $N_{1,60f}$ value at the depth in question is around 34. Since this value is greater than 30, it can be directly inferred that there is no liquefaction potential at this depth.

Finally, Table 4 summarizes all the analysis procedures. This table lists liquefaction resistance (τ_R), average cyclic shear stress (τ_{av}), and factors of safety against liquefaction phenomena (FS) for both GWT conditions. The layers where FS is less than 1.1 are considered as soils with potential liquefaction risk, as stated in TBEC (Republic of Türkiye 2018). According to TBEC (Republic of Türkiye 2018), where the groundwater level is located at

Table 4 Factor of safety against liquefaction for both GWT conditions

Depth (m)	1.5	3.0	4.5	6.0	7.5	9.0	10.5	12.0	13.5	15.0	16.5	18.0	19.5
GWT at −10 m													
τ_{av} (kPa)	6.05	11.97	18.93	24.93	30.79	36.50	43.55	47.87	51.60	54.75	57.30	62.67	64.12
τ_{R} (kPa)	3.68	4.93	8.89	12.14	13.32	22.33	33.99	36.73	40.55	49.09	60.20	67.79	107.43
F.S. (−)	NL	NL	NL	NL	NL	NL	0.78	0.767	0.786	NL	1.0506	1.0817	1.6756
GWT at the surface													
τ_{av} (kPa)	6.46	12.77	20.11	26.49	32.72	38.78	45.98	50.19	53.82	56.85	59.30	64.56	65.90
τ_{R} (kPa)	1.52	2.04	5.05	7.38	7.62	13.77	23.74	26.62	31.00	40.84	58.50	65.00	NL
F.S. (−)	0.24	0.16	0.25	NL	0.23	NL	0.52	0.53	0.58	NL	0.99	1.01	NL

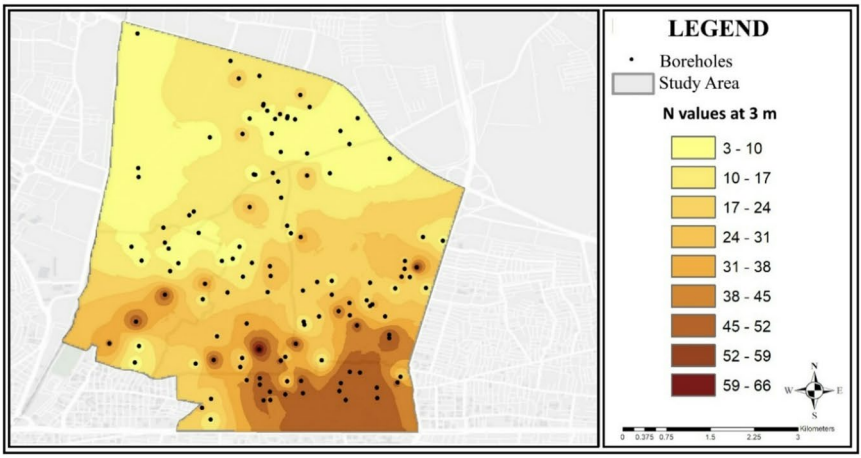
the current level of −10 m, it is directly accepted that there is no liquefaction risk for the first 10 m, as it is above the GWT. However, as soon as the GWT level is considered to be at the surface, there is a high level of liquefaction risk in the whole layer at the first 10 m. This shows how important it is to determine the GWT level correctly and to monitor seasonal fluctuations in the GWT level.

These illustrative calculations are performed in the same systematic procedure for all other boreholes used in the study, and the mapping process is carried out based on the minimum FS values at each borehole location.

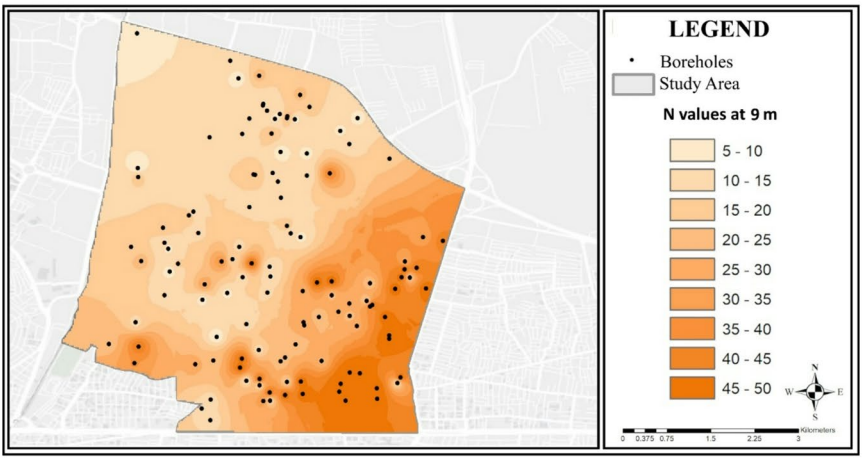
4.2 Mapping the Spatial distribution of SPT blow numbers and GWT depths

Geographic Information Systems (GIS) are used to evaluate the spatial distribution of the data obtained from the boreholes. Firstly, the spatial distributions of SPT-N (Standard Penetration Test) values for three different depth levels (3 m, 9 m, and 15 m) are obtained and illustrated through mapping as shown in Fig. 4. These maps showing the distribution represent low SPT values in red color and high SPT values in blue color. Intermediate values are represented by orange, yellow, and green tones from low to high, respectively. According to the SPT distribution maps presented in Fig. 4, it is observed that higher SPT-N values are obtained for all three depth levels in the southern parts of the study area. This indicates that the soil layers in these regions are denser and therefore the liquefaction potential is lower. In other words, there are more resistant soil conditions in the southern regions.

Secondly, a map presenting the distribution of the depth of the current groundwater level in the study area is presented in Fig. 5. In this map, the areas where the depth of the groundwater level is high from the surface are shown in blue color, and the areas where the depth is relatively lower are shown in red color. The intermediate depth levels are represented by green, yellow, and orange tones from high to low depths, respectively. According to the distribution presented by the map, it is clearly seen that the groundwater level is located deeper in the southern regions. This indicates that the saturation condition of the ground, which is one of the first conditions for liquefaction, is less likely to be reached in these regions.



(a)



(b)



Fig. 4 Spatial distribution of SPT–N values at **a** 3 m **b** 9 m **c** 15 m

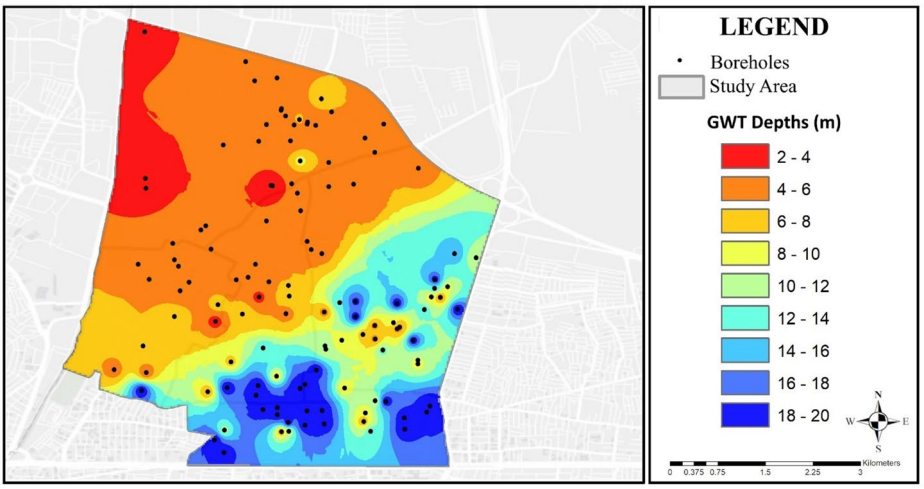


Fig. 5 Spatial distribution of GWT depth in the study area

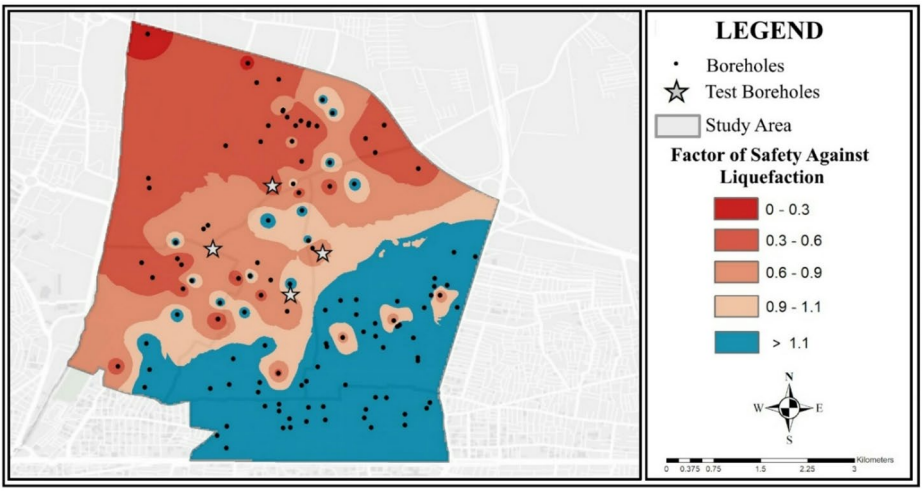
4.3 Mapping the Spatial distribution of the safety factor against liquefaction

In this section, safety factor (FS) maps prepared for the evaluation of liquefaction potential, considering two different groundwater level (GWL) scenarios (Fig. 6). The first scenario represents the current groundwater level conditions (Fig. 6a), while the second scenario assumes the most unfavorable situation where groundwater is at the surface level (Fig. 6b). This approach is adopted to be on the safe side, as groundwater level data is subject to seasonal variability and may reach higher levels in the future.

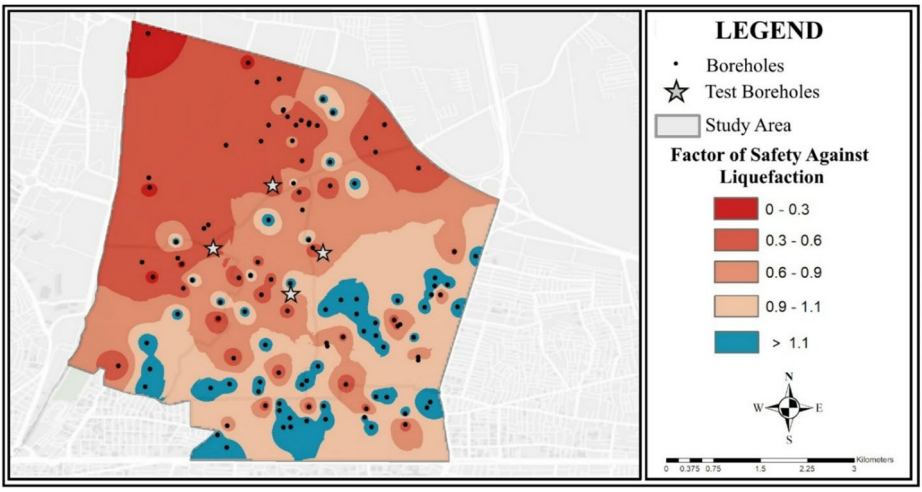
In both scenarios, only the minimum FS values calculated in the soil layers below the groundwater level are considered. Maps are generated to reflect the spatial distribution of these values and made visually interpretable. Regions with FS > 1.1 are shown in blue tones, while regions with FS < 1.1 are marked in red tones. As the safety factor decreases, the red tone gets darker, so that the degree of liquefaction risk can be visually distinguished. The map of the current condition shown in Fig. 6a reveals that the safety factors are mostly above 1.1, especially in the southern parts of the study area, and that these regions are relatively safe in terms of liquefaction. However, in the map of the worst possible scenario presented in Fig. 6b, the liquefaction hazard is not observed in only rare areas, and FS values are below the critical limit in the whole study area. This indicates that possible rises in the water level may seriously increase the risk of liquefaction. Considering both maps together, a decrease in FS is observed from south to north. Therefore, it is concluded that the liquefaction risk increases in the north direction. This finding is also supported by the observation of higher SPT-N values in the southern regions in the distribution maps previously generated for different depths. Therefore, the findings are consistent with each other.

4.4 Evaluation of errors in IDW interpolation

The accuracy of the IDW interpolation method used in creating liquefaction risk maps is tested by excluding four borehole points selected at the center of the study area (shown at



(a)



(b)

Fig. 6 Spatial distribution of FS against liquefaction for GWT at **a** the current level **b** the surface

locations marked with a star symbol in Fig. 6) from the analysis for testing purposes. Table 5 compares the measured values for these four points with the values estimated using the IDW method, and also calculates the error (Error), absolute error (|Error|), squared error ($Error^2$), and relative error (Rel. Error) values. Point-based evaluations show that the estimates generally converge with the measurements, but there are deviations at a certain level. This indicates spatial estimation errors inherent in the interpolation process.

Table 6 presents summary error statistics and compares two different GWL scenarios. Mean absolute error (MAE = 0.133), mean squared error (MSE = 0.027), and root mean squared error (RMSE = 0.165) values obtained at the current GWL indicate that IDW interpolation exhibits acceptable performance. The low standard error (0.113) supports

Table 5 Error parameters for the four test points at two different GWL scenarios

GWL scenarios	At the current level				At the surface			
Borehole no. (−)	10	48	55	71	10	48	55	71
Measured FS (−)	0.4	0.49	0.75	0.76	0.4	0.37	0.63	0.56
Calculated FS (−)	0.42	0.72	0.98	0.81	0.41	0.55	0.93	0.64
Error (−)	0.02	0.23	0.23	0.05	0.01	0.18	0.3	0.08
|Error| (−)	0.02	0.23	0.23	0.05	0.01	0.18	0.3	0.08
$Error^2$ (−)	0.0004	0.0529	0.0529	0.0025	0.0004	0.0324	0.09	0.0064
Rel. Error (%)	5.0	46.9	30.7	6.6	2.5	48.6	47.6	14.3

Table 6 Summary of error statistics at two different GWL scenarios

GWL scenarios	At the current level	At the surface
ME (−)	0.133	0.143
MAE (−)	0.133	0.143
MSE (−)	0.027	0.032
RMSE (−)	0.165	0.18
Std. Dev. of Error (−)	0.113	0.126
Rel. Error (%)	22.3	28.3

the method's stable estimation power under current conditions. However, in the scenario where the GWL is assumed at the surface, an increase is observed in all error criteria (e.g., RMSE = 0.180; Rel. Error = 28.3%), clearly demonstrating that hydrogeological assumptions increase the uncertainty in liquefaction risk predictions. The reason for this increase can be explained by the fact that the SPT-N values used in liquefaction analyses depend on the current saturation conditions. When the groundwater level is assumed to rise, the direct use of the same N values for saturated conditions reduces the representativeness of the drilling points and increases the error rates. Therefore, the differences observed in the error analysis reflect epistemic uncertainties caused by scenario assumptions rather than structural limitations of IDW interpolation.

4.5 Determination of optimum borehole number based on epistemic uncertainty

This section of the study examines the effect of reducing the number of boreholes on IDW interpolation accuracy and discusses the optimal number of boreholes using the epistemic uncertainty approach. The results demonstrate the possibility of producing reliable estimates with minimal data.

Figure 7 shows the spatial distribution of borehole locations, boreholes extracted from the analysis, and test boreholes used solely for testing purposes. The symbols and colors used in the figure represent different stages. Black stars indicate four test borehole locations excluded from the analysis to test the accuracy of the IDW interpolation. Yellow pentagons (Borehole 101–119) represent the boreholes extracted from the analysis during the reduction process from 119 boreholes to 100 boreholes. Blue triangles (Borehole 81–100) show the boreholes extracted when reducing from 100 boreholes to 80 boreholes. The green squares (Borehole 61–80) represent the boreholes excluded from analysis during the reduction from 80 to 60 boreholes. The red circles (Borehole 1–60) indicate the basic 60 borehole points used in all scenarios.

The results of the epistemic uncertainty analysis for different YASS scenarios are summarized in Tables 7 and 8. Accordingly, under the current groundwater level conditions (Table 7), the error metrics obtained from 119 borehole points (e.g., MAE = 0.133, RMSE = 0.165, RelError = 22.3%) are largely preserved in the analyses performed with 100 borehole points, and even a decrease in the relative error rate (19%) is observed. However, when the number of boreholes is reduced to 80, both absolute and quadratic error values increase, and error values rise significantly, especially when the number of boreholes is reduced to 60 (e.g., RMSE = 0.299, RelError = 50.7%). A similar trend is observed in the scenario where the groundwater level is assumed to be at the surface (Table 8). Under this condition, the error metrics remain at acceptable levels up to 100 borehole points (MAE = 0.155, RMSE = 0.195, RelError = 25.9%), but the error rates gradually increase in the analyses performed with 80 and 60 borehole points, reaching a high error rate at 60 points (RMSE = 0.290, RelError = 53.6%).

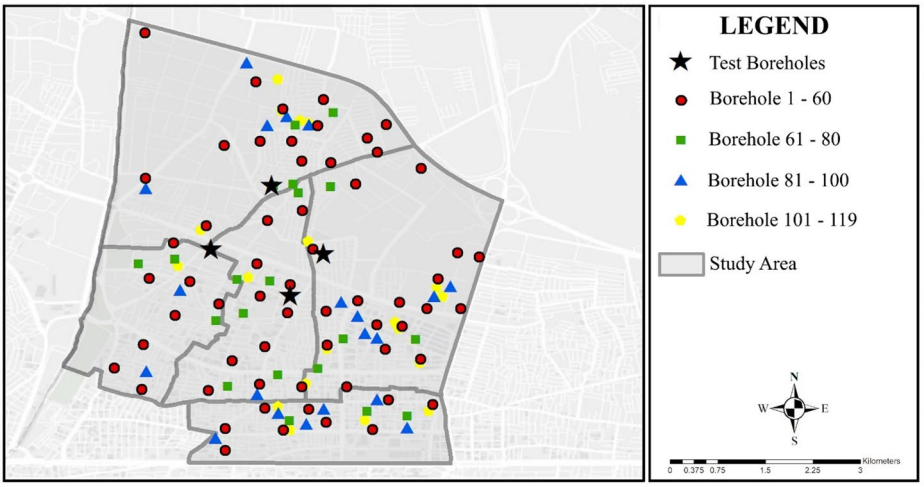


Fig. 7 Display of borehole points extracted at different stages within the epistemic uncertainty approach

Table 7 Summary of error statistics for various numbers of borehole points at the current GWL

Number of borehole points	119	100	80	60
ME (−)	0.133	0.108	0.113	0.245
MAE (−)	0.133	0.133	0.143	0.265
MSE (−)	0.027	0.027	0.031	0.09
RMSE (−)	0.165	0.165	0.176	0.299
Std Dev of Error (−)	0.113	0.144	0.157	0.199
Rel. Error (%)	22.3	19.0	20.2	50.7

Table 8 Summary of error statistics for various numbers of borehole points at the highest GWL

Number of borehole points	119	100	80	60
ME (−)	0.143	0.12	0.128	0.233
MAE (−)	0.143	0.155	0.168	0.263
MSE (−)	0.032	0.038	0.044	0.084
RMSE (−)	0.18	0.195	0.209	0.29
Std. Dev. of Error (−)	0.126	0.177	0.191	0.199
Rel. Error (%)	28.3	25.9	28.2	53.6

5 Discussion

In this study, the liquefaction potential of five neighborhoods (Millet, Vatan, Kazımkarabekir, Yunusemre, and Duaçınarı) located in the Yıldırım district of Bursa province is evaluated in accordance with the Turkish Building Earthquake Code (TBEC 2018), and GIS-based spatial hazard maps are produced. The primary data used in the study are SPT results and laboratory tests obtained from 123 borehole points. Using these data, the liquefaction safety factor (FS) distribution is estimated using the IDW (Inverse Distance Weighted) interpolation method and evaluated for two different groundwater level (GWL) scenarios: current conditions and the worst-case scenario, where the groundwater level is at the surface.

The findings show that the groundwater level has a determining effect on the liquefaction potential. Under the current water level conditions, there is no liquefaction potential in Duaçınarı Neighborhood. On the other hand, when the water level is assumed to be at the surface, liquefaction risk is observed in most parts of the study area, including this region. This indicates that the groundwater level may rise over time due to seasonal and meteorological effects, and accordingly, risk analyses should be addressed with a dynamic approach. Therefore, it is necessary to periodically measure the groundwater level at different times, especially before construction and ground improvement works.

The study also evaluated the accuracy of the IDW interpolation method using error analysis with four test borehole points. The error metrics obtained (ME, MAE, MSE, RMSE,

standard deviation, and relative error) show that the model provides reasonable predictions in both GWL scenarios. However, while the relative error is 22.3% under current conditions, it increases to 28.3% when GWL is present at the surface. This difference indicates that modeling the groundwater level at levels different from its current state may create additional uncertainties in the predictions. Consequently, it is concluded that the SPT-N values used in liquefaction analyses are sensitive to the current wetness conditions, and therefore, water level assumptions can directly affect the model results.

To assess epistemic uncertainty, the IDW interpolation using 119 borehole points is repeated with different borehole counts (100, 80, and 60 points), and the change in error values is evaluated. The results show that error values remained at an acceptable level up to 100 borehole points in both YASS scenarios, but when the number of points drops to 80 and especially 60, there is a significant increase in both absolute and relative error values (Tables 7 and 8). In particular, the relative error exceeding 50% when reduced to 60 points indicates that reducing the number of points below this level seriously weakens the reliability of the model. This finding suggests that the optimal number of borehole points in the study can be considered to be at least 100. However, this number is specific to the study and may be influenced by factors such as point distribution density and the heterogeneity of the study area.

Methodologically, the IDW method is preferred in this study; however, the reliability of the method may be limited in areas with low data density. More complex interpolation methods, such as Kriging or TIN, are also used as alternatives in the literature. Comparing these methods in future studies may provide a clearer picture of the uncertainties in liquefaction potential. Similarly, SPT results are used as the primary data source in this study due to their widespread use and accessibility. However, methods that provide more continuous and high-resolution data, such as CPT (Cone Penetration Test), are also thought to make significant contributions to liquefaction analysis.

Additionally, within the context of this study, the maps are generated with ArcGIS software. However, it is known that different GIS software, such as AtlasGIS, Idrisi, Geomap, MapInfo, and recently artificial intelligence-based spatial modeling applications, are also used for similar operations in the literature. Processing the obtained data on such alternative platforms and comparing them with ArcGIS-based results will contribute to methodological diversity.

Consequently, the GIS-based liquefaction hazard maps obtained in this study can be considered as an important decision support tool for local governments, ground investigation firms, and urban planners. Such studies are especially instructive in reducing disaster risks, determining urban transformation areas, and evaluating development plans with respect to ground safety. However, all these findings should be carefully assessed considering the limitations in site characterization, data density, seasonal variability, and the effects of method choices.

6 Conclusion

This study assessed liquefaction potential based on 123 borehole data points collected in five neighborhoods (Millet, Vatan, Kazımkarabekir, Yunusemre, and Duaçınarı) in the Yıldırım district of Bursa province, within the scope of TBEC (2018). GIS-based risk maps prepared

using IDW interpolation are compared for the current groundwater level and the most unfavorable scenario where the water level is assumed to be at the surface. The findings show that the groundwater level is a decisive factor in liquefaction potential. It is revealed that in areas where the risk is limited under current conditions, the risk increases significantly in the scenario where water is assumed to be at the surface.

The reliability of the results obtained is evaluated through error analyses and epistemic uncertainty studies. The error analyses show that the interpolation analyses contain acceptable errors under both GWL scenarios, although higher error metrics are observed under the condition that GWL is accepted on the surface. Another original contribution of the study is the evaluation of the optimal number of wells using the epistemic uncertainty approach. The comparisons made showed that low borehole density increases error values and that the reliability of the results decreases, especially when the number of borehole points falls below 60. When approximately 100 borehole points are used, error values remain at an acceptable level, demonstrating that spatial distribution plays a critical role in the analyses.

In conclusion, this study not only assessed the current situation but also presented a comprehensive approach to liquefaction potential, considering the worst-case scenario and uncertainties related to data density. The findings indicate that the groundwater level, which may vary due to seasonal fluctuations, should be monitored regularly, and that it would be appropriate to consider the worst-case conditions in risk analyses. The use of alternative data sources, such as CPT, and different spatial modeling techniques in future studies will both increase the accuracy of liquefaction assessments and provide robust decision support mechanisms for disaster management and urban planning.

Author contributions Onur Gurbuz took part in the data acquisition and analysis of the article. Ahmet Talha Gezgin took an active role in the writing of the study from start to finish and interpretation of the results. All authors approved the final version of the manuscript.

Funding Open access funding provided by the Scientific and Technological Research Council of Türkiye (TÜBİTAK).

Data availability Data may be shared by the corresponding author upon reasonable request.

Declarations

Conflict of interest The authors declare that there is no conflict of interest related to this study.

Ethical approval Ethical approval is not required as this study was not conducted on human or animal subjects.

Publication consent The authors agree to the publication of the manuscript.

Open Access This article is licensed under a Creative Commons Attribution 4.0 International License, which permits use, sharing, adaptation, distribution and reproduction in any medium or format, as long as you give appropriate credit to the original author(s) and the source, provide a link to the Creative Commons licence, and indicate if changes were made. The images or other third party material in this article are included in the article's Creative Commons licence, unless indicated otherwise in a credit line to the material. If material is not included in the article's Creative Commons licence and your intended use is not permitted by statutory regulation or exceeds the permitted use, you will need to obtain permission directly from the copyright holder. To view a copy of this licence, visit http://creativecommons.org/licenses/by/4.0/.

References

Akyol N, Akıncı A, Eyidogan H (2002) Site amplification of S-waves in bursa City and its vicinity, Northwestern turkey: comparison of different approaches. Soil Dyn Earthq Eng 22:579–587

Ali S, Rahman A (2022) Development of a kriging-based regional flood frequency analysis technique for South-East Australia. Nat Hazards 114:2739–2765. https://doi.org/10.1007/s11069-022-05488-4

Ansary MA, Ansary M, Ahamed S (2024) Liquefaction potential assessment of the DMDP area of Bangladesh using CPT-based methods. Nat Hazards 120:9777–9808. https://doi.org/10.1007/s11069-024-06586-1

Arango I (1996) Magnitude scaling factors for soil liquefaction evaluations. J Geotech Eng 122:929–936

Atlasbig https://atlasbig.com.tr/bursa-yildirimin-mahalleleri

Aytaş Z, Alpaslan N, Özçep F (2023) Evaluation of liquefaction potential by standard penetration test and shear wave velocity methods: a case study. Nat Hazards 118:2377–2417. https://doi.org/10.1007/s11069-023-06093-9

Başarı E (2003) Dynamic Soil Behaviour Analysis of Soils in Bursa City Centre (In Turkish). Master Thesis, Celal Bayar University

Bayramoğlu M, Özel S (2024) The analysis and mapping of an urban planning area in risk and hazard dimensions using earthquake-MASW-VES data: the case of Yenişehir (Bursa)Turkey. Nat Hazards https://doi.org/10.1007/s11069-024-06855-z.

Bazaraa ARS (1967) Use of the standard penetration test for estimating settlements of shallow foundations on sand. Doctor of Philosophy, University of Illinois at Urbana

Bourenane H, Bouhadad Y, Tas M (2018) Liquefaction hazard mapping in the City of Boumerdès, Northern Algeria. Bull Eng Geol Environ 77:1473–1489. https://doi.org/10.1007/s10064-017-1137-x

Burrough PA, McDonnell RA, Lloyd CD (2015) Principles of geographical information systems. Oxford University Press, Oxford, UK

Cetin KO, Seed RB, Kayen RE et al (2018) SPT-based probabilistic and deterministic assessment of seismic soil liquefaction triggering hazard. Soil Dyn Earthq Eng 115:698–709. https://doi.org/10.1016/j.soildyn.2018.09.012

Fardad Amini P, Noorzad R (2018) Energy-based evaluation of liquefaction of fiber-reinforced sand using Cyclic triaxial testing. Soil Dyn Earthq Eng 104:45–53. https://doi.org/10.1016/j.soildyn.2017.09.026

Gibbs HJ, Holtz WG (1957) Research on determining the density of sands by spoon penetration testing. In: 4th International conference on soil mechanics and foundation engineering. London

Idriss IM (1990) Response of soft soil sites during earthquakes. In: Bolton H (eds) Seed memorial symposium, California, ABD

Idriss IM, Boulanger RW (2008) Soil liquefaction during earthquakes. EARTHQUAKE ENGINEERING RESEARCH INSTITUTE, Oakland, California, USA

Khashila M, Hussien MN, Karray M, Chekired M (2021) Liquefaction resistance from Cyclic simple and triaxial shearing: a comparative study. Acta Geotech 16:1735–1753. https://doi.org/10.1007/s11440-020-01104-6

Kramer SL, Stewart JP (2025) Geotechnical earthquake engineering. CRC, Boca raton

Liao S, Whitman RV (1986) Overburden correction factors for SPT in sand. J Geotech Eng 112:373–377

Memisoglu Baykal T (2025) Performance assessment of GIS-based Spatial clustering methods in forest fire data. Nat Hazards. https://doi.org/10.1007/s11069-025-07135-0

Meshram SG, Singh VP, Kisi O, Meshram C (2021) Soil erosion modeling of watershed using cubic, quadratic and Quintic splines. Nat Hazards 108:2701–2719. https://doi.org/10.1007/s11069-021-04796-5

Mhaske SY, Choudhury D (2010) GIS-based soil liquefaction susceptibility map of Mumbai City for earthquake events. J Appl Geophy 70:216–225. https://doi.org/10.1016/j.jappgeo.2010.01.001

Park SS, Nong ZZ, Lee DE (2020) Effect of vertical effective and initial static shear stresses on the liquefaction resistance of sands in Cyclic direct simple shear tests. Soils Found 60:1588–1607. https://doi.org/10.1016/j.sandf.2020.09.007

Poddar P, Ojha S, Gupta MK (2023) Probabilistic and deterministic-based approach for liquefaction potential assessment of layered soil. Nat Hazards 118:993–1012. https://doi.org/10.1007/s11069-023-06031-9

Puri N, Jain A, Nikitas G et al (2020) Dynamic soil properties and seismic ground response analysis for North Indian seismic belt subjected to the great Himalayan earthquakes. Nat Hazards 103:447–478. https://doi.org/10.1007/s11069-020-03995-w

Rawat A, Kumar D, Chatterjee RS, Kumar H (2022) A GIS-based liquefaction susceptibility mapping utilising the morphotectonic analysis to highlight potential hazard zones in the East Ganga plain. Environ Earth Sci https://doi.org/10.1007/s12665-022-10468-9

Republic of Türkiye M of EU and CC (2018) Turkish Building Earthquake Code (TBEC-2018). Turkey

Robertson PK, Wride CE (1998) Evaluating Cyclic liquefaction potential using the cone penetration test. Can Geotech J 35:442–459

Seed HB, Idriss IM (1967) Analysis of soil liquefaction: Niigata earthquake. J Soil Mech Found Div 93:83–108
Seed HB, Idriss IM (1971) A simplified procedure for evaluating soil liquefaction potential. J Soil Mech Found Div 97:1249–1273
Seed HB, Idriss IM (1982) Ground motions and soil liquefaction during earthquakes. Earthquake Engineering Research Institute
Seed HB, Arango I, Chan CK (1975) Evaluation of soil liquefaction potential for level ground during earthquakes. ASCE National Convention
Seed HB, Tokimatsu K, Harder LF, Chung RM (1985) Influence of SPT procedures in soil liquefaction resistance evaluations. J Geotech Eng 111:1425–1445
Sett S, Chattopadhyay KK, Ghosh A (2023) Liquefaction hazard mapping and relationship between probability of liquefaction and factor of safety for Kolkata city, India. Nat Hazards 118:347–376. https://doi.org/10.1007/s11069-023-06007-9
Shynkarenko A, Kremer K, Stegmann S et al (2022) Geotechnical characterization and stability analysis of subaqueous slopes in lake Lucerne (Switzerland). Nat Hazards 113:475–505. https://doi.org/10.1007/s11069-022-05310-1
Sitharam TG, Anbazhagan P, Mahesh GU (2007) 3-D subsurface modelling and preliminary liquefaction hazard mapping. of Bangalore City Using SPT Data and GIS
Tabban A (2000) Geology and earthquake status of cities (in Turkish). Jeoloji Mühendisleri Odası Yayınları, Ankara
Teng WC (1962) Foundation design. Prentice-Hall Inc, Essex
Tokimatsu K, Yoshimi Y (1983) Empirical correlation of soil liquefaction based on SPT N-value and fines content. Soils Found 23:56–74
Tosun H, Seyrek E, Orhan A et al (2011) Soil liquefaction potential in Eskişehir, NW Turkey. Nat Hazards Earth Syst Sci 11:1071–1082. https://doi.org/10.5194/nhess-11-1071-2011
Turkish Statistical Institute (TSI) (2025) Address based population registration system results, 2024. Ankara, Turkey
Yanto AA, Santoso PB, Sumiyanto (2022) Landslide susceptible areas identification using IDW and ordinary kriging interpolation techniques from hard soil depth at middle Western central Java, Indonesia. Nat Hazards 110:1405–1416
Youd TL, Idriss IM (2001) Liquefaction resistance of soils: summary report from the 1996 NCEER and 1998 NCEER/NSF workshops on evaluation of liquefaction resistance of soils. J Geotech GeoEnviron Eng 127: 297–313.
Zhuang H, Wang R, Chen G et al (2018) Shear modulus reduction of saturated sand under large liquefaction-induced deformation in Cyclic torsional shear tests. Eng Geol 240:110–122. https://doi.org/10.1016/j.enggeo.2018.04.018

Publisher's note Springer Nature remains neutral with regard to jurisdictional claims in published maps and institutional affiliations.

Authors and Affiliations

Ahmet Talha Gezgin[1] · **Onur Gurbuz**[1]

✉ Ahmet Talha Gezgin
ahmettalhagezgin@uludag.edu.tr

[1] Department of Civil Engineering, Bursa Uludag University, Nilüfer, Bursa, Turkey